Available online at www.sciencedirect.com

SciVerse ScienceDirect

Acta Materialia 59 (2011) 7189–7198

Acta MATERIALIA

www.elsevier.com/locate/actamat

Strain effect on phase transitions of $BaTiO_3$ nanowires

J.J. Wang [a,b,*], E.A. Eliseev [c], X.Q. Ma [a], P.P. Wu [a,b], A.N. Morozovska [c], Long-Qing Chen [b]

[a] Department of Physics, University of Science and Technology Beijing, Beijing 100083, People's Republic of China
[b] Department of Materials Science and Engineering, Pennsylvania State University, University Park, PA 16802, USA
[c] National Academy of Sciences of Ukraine, 03028 Kiev, Ukraine

Received 5 April 2011; received in revised form 10 August 2011; accepted 11 August 2011
Available online 23 September 2011

Abstract

The effects of strain on the phase transitions of $BaTiO_3$ nanowires taking into account three components of polarization are studied by thermodynamic analysis based on the Landau theory. Similar to the strain effect on phase transitions in thin films, the mismatch strain between the nanowire and substrate governs the Curie temperature. The complete misfit strain–temperature phase diagram shows six stable ferroelectric phases for $BaTiO_3$ nanowires under different strain and temperature conditions.
Published by Elsevier Ltd. on behalf of Acta Materialia Inc.

Keywords: Nanocrystalline materials; Phase transformations; Ferroelectricity; Phenomenological simulation

1. Introduction

Nanoscale ferroelectric structures have been explored to increase the storage density of non-volatile ferroelectric random access memories [1,2]. For example, ferroelectric nanowires (FNWs) are being considered as a new media for next-generation ultrahigh-density computer memory [3–5]. Ferroelectric nanostructures with size and shape control [6–10] have been synthesized [11–15]. For instance, Mao et al. synthesized single-crystalline $BaTiO_3$ nanowires using a simple one-step solid-state chemical reaction [8]. Urban et al. showed that crystalline nanorods composed of $BaTiO_3$ and $SrTiO_3$ with a cubic perovskite structure could be synthesized via a solution-based decomposition of bimetallic alkoxide precursors [9].

To characterize FNWs, Wang et al. employed piezoresponse force microscopy to study the polarization switching by directly applying an electric bias to a $BaTiO_3$ nanowire [11]. Yun et al. demonstrated the writing of nonvolatile electric polarization domains using scanning probe microscopy (SPM) on $BaTiO_3$ nanowires [12]. Spanier et al. used SPM to measure the ferroelectric phase transition temperatures in individual $BaTiO_3$ nanowires, showing a $1/d_{NW}$ dependence where d_{NW} is the wire diameter. These experiments established a resolution limit for a local domain of as little as 3 nm [14].

The size effects and ferroelectric behaviors of nanowires have also been studied theoretically, including by ab initio methods [5,16–18], molecular dynamics (MD) simulation [19,20] and the Landau–Ginzburg–Devonshire (LGD) theory [21–24]. For example, Naumov and Fu performed ab initio studies of ferroelectric nanoscale disks and rods of technologically important $Pb(Zr, Ti)O_3$ solid solutions, and demonstrated a number of novel phase transitions in zero-dimensional ferroelectric nanoparticles [16]. Pilania et al. determined the critical diameters for the development of spontaneous polarization parallel and perpendicular to the axis direction of $BaTiO_3$ nanowires; these diameters were 1.2 and 1.6 nm, respectively [17]. Shimada et al.

* Corresponding author at: Department of Materials Science and Engineering, Pennsylvania State University, University Park, PA 16802, USA. Tel.: +1 8148650389.
E-mail address: wjj8384@gmail.com (J.J. Wang).

1359-6454/$36.00 Published by Elsevier Ltd. on behalf of Acta Materialia Inc.
doi:10.1016/j.actamat.2011.08.015

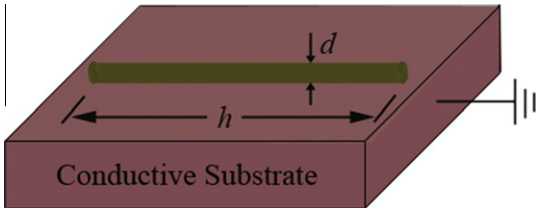

Fig. 1. Model of $BaTiO_3$ nanowire grown on a conductive substrate used in this work; d and h denote the diameter and length of the nanowire, respectively. The electric boundary condition between the two head faces is assumed to be short-circuited as the head–tail distance is remote. The misfit strain u_s induced by the substrate is along the wire direction and can be described as $u_s = (a_s - a_c)/a_c$.

investigated the role of axial tensile strain on the nanowires, and the ferroelectricity of $PbTiO_3$ nanowires by means of ab initio calculations [18]. Using the MD method, Zhang et al. studied the polarization distribution, hysteresis behavior and the Curie temperature of $BaTiO_3$ nanowires. They determined that the two critical diameters for the existence of polarization parallel and perpendicular to the axis direction are 0.8 and 1.2 nm, respectively [19]. Zhang et al. also investigated the strain and size effects on the ferroelectric behaviors of $BaTiO_3$ nanowires using MD [20]. Using the direct variational method and assuming the polarization is along the axial direction of the nanorods and nanowires, Morozovska et al. solved the Euler–Lagrange equations derived from the LGD free energy expression to obtain the approximate analytical expression for the dependence of the Curie temperature on size, polarization gradient coefficient, extrapolation length, effective surface, tension and electrostriction coefficient [23]. Using a similar method and based on the assumption that the polarization is along the radial direction, Hong et al. investigated the size-dependent ferroelectric properties of $BaTiO_3$ nanowires, including the Curie temperature and the hysteresis loop [21].

In this work, we study the size and strain effects on phase transitions of $BaTiO_3$ nanowires using a modified Landau potential which takes into account the low-temperature quantum effect as well as pressure-dependent Landau coefficients [25]. Based on the fact reported by Wang et al. that the one-dimensional and stable ferroelectric monodomain might exist in single-crystalline $BaTiO_3$ nanowires [15], single-domain structures are assumed in our calculation for simplicity. We consider nanowires epitaxally grown on conductive substrates,[13,15] and the short-circuit electric boundary condition is assumed along the axis of nanowire, as shown in Fig. 1.

2. Thermodynamic model

We use $g_{\mathrm{LGD}}(\vec{P}, T)$ to represent the stress-free bulk Gibbs free energy density function of a ferroelectric crystal at a given polarization ($\vec{P}$) and temperature (T). The total Gibbs free energy (G) of a finite ferroelectric crystal containing inhomogeneous polarization distribution is then written as [26,27]:

$$G(\sigma, T) = \iiint_V (g_{\mathrm{LGD}} + g_{\mathrm{elastic}} + g_{\mathrm{grad}} + g_{\mathrm{electric}})dV + \iint_A g_{\mathrm{surface}}dA, \quad (1)$$

with $g_{LGD}(\vec{P}, T)$ represented by a Landau potential:

$$\begin{aligned} g_{\mathrm{LGD}} = {} & \alpha_1(P_1^2 + P_2^2 + P_3^2) + \alpha_{11}(P_1^4 + P_2^4 + P_3^4) \\ & + \alpha_{12}(P_1^2P_2^2 + P_1^2P_3^2 + P_2^2P_3^2) + \alpha_{111}(P_1^6 + P_2^6 \\ & + P_3^6) + \alpha_{112}[P_1^4(P_2^2 + P_3^2) + P_2^4(P_1^2 + P_3^2) \\ & + P_3^4(P_1^2 + P_2^2)] + \alpha_{123}P_1^2P_2^2P_3^2 + \alpha_{1111}(P_1^8 + P_2^8 \\ & + P_3^8) + \alpha_{1122}(P_1^4P_2^4 + P_1^4P_3^4 + P_2^4P_3^4) \\ & + \alpha_{1112}[P_1^6(P_2^2 + P_3^2) + P_2^6(P_1^2 + P_3^2) + P_3^6(P_1^2 \\ & + P_2^2)] + \alpha_{1123}(P_1^4P_2^2P_3^2 + P_1^2P_2^4P_3^2 + P_1^2P_2^2P_3^4), \end{aligned} \quad (2)$$

where the coefficients were fitted to bulk properties at zero stress by considering the low-temperature quantum effects [25], and P_i is the ith component of polarization. The elastic energy density g_{elastic} is given by:

$$\begin{aligned} g_{\mathrm{elastic}} = {} & -\frac{1}{2}s_{11}(\sigma_1^2 + \sigma_2^2 + \sigma_3^2) - s_{12}(\sigma_1\sigma_2 + \sigma_1\sigma_3 \\ & + \sigma_2\sigma_3) - \frac{1}{2}s_{44}(\sigma_4^2 + \sigma_5^2 + \sigma_6^2) - Q_{11}(\sigma_1P_1^2 \\ & + \sigma_2P_2^2 + \sigma_3P_3^2) - Q_{44}(\sigma_4P_2P_3 + \sigma_5P_1P_3 \\ & + \sigma_6P_1P_2) \\ & - Q_{12}\left[\sigma_1(P_2^2 + P_3^2) + \sigma_2(P_1^2 + P_3^2) + \sigma_3(P_1^2 + P_2^2)\right], \end{aligned} \quad (3)$$

where σ_i is the ith component of stress in Voigt notation, s_{11}, s_{12} and s_{44} are the elastic compliance constants of a cubic phase, and Q_{11}, Q_{12} and Q_{44} are the corresponding electrostrictive coefficients. The compliance and electrostrictive constants can be obtained by experimental measurements or first-principles calculations [28,29]. The gradient energy density g_{grad} can be written as $g_{\mathrm{grad}} = \frac{1}{2}D_{ij}P_{i,j}P_{i,j}$, where D_{ij} are the gradient energy coefficients [30]. For a ferroelectric with homogeneous polarization, g_{grad} is zero. The matrix D_{ij} of the gradient energy coefficients is positively defined for most ferroelectrics, except the incommensurate ones.

The electrostatic energy density g_{electric} includes contributions from both an external applied field and the depolarization field that exists in the spatial regions with $\mathrm{div}\mathbf{P} \neq 0$, including surfaces, interfaces and in the vicinity of domain walls. For the short-circuit electric boundary condition, the contribution of applied external field to total electrostatic energy should also be zero. The depolarization field along the wire direction can be estimated by $E_3^{\mathrm{D}} \approx -\lambda(P_3 - q_e)/\varepsilon_b$, where q_e is the compensation charge density at the left and right electrodes, and $\varepsilon_b = \varepsilon_0\varepsilon_{33}^b$ is the background permittivity [31]. Factor λ can be estimated using the relation $\lambda \approx 1/\lfloor 1 + (h/2d)^2 \rfloor$ where h is the length, and d the diameter of the nanowires [23,24]. In the case of FNWs, $h \gg d$, the corresponding value of λ equals zero [23,32], and thus the depolarization

E_3^D can be neglected in all subsequent considerations. The perpendicular-to-axis polarization components P_1 and P_2 will induce a depolarization field $\overrightarrow{E}_{\perp}^{D}$, which can be obtained by solving the electrostatic equilibrium equation $\nabla \bullet (\varepsilon_b \overrightarrow{E}_{\perp}^{D} + \overrightarrow{P}_{\perp}) = 0$ [1,33–37]. Wang et al. obtained that the radial depolarization field is $E_{\perp}^{D} \approx -\frac{2l_d}{\varepsilon_0 \varepsilon_b d} P_{\perp}$, where ld is effective screening length, which characterizes the effective thickness of the double electric layer formed by the bound and free charges [37]. A nanowire model with three layers including the isotropic nanowire core, external screening layer and the ambient medium layer was proposed to derive the more rigorous estimation for $E_{\perp}^{D}$ in the Appendix A. We used the results of $E_{\perp}^{D} = -\frac{P_{\perp}}{\varepsilon_0 \varepsilon_b}\eta$ with the assumption of homogeneous polarization distribution inside the wire. The form of factor η depends on the boundary conditions at the nanowire surface as well as on its ambient (i.e. on the surrounding matrix permittivity and conductivity), as discussed in Appendix A. Here we show (see Fig. A1) that η can be tuned to be as small as necessary by high $\varepsilon_e, \varepsilon_s$, etc. It can be seen from Fig. A1c and d, that the contribution of the depolarization field to the total energy is negligibly small (i.e. $|\varepsilon_0 \varepsilon_b \alpha_1(T)/\eta(R)| >> 1$) in the actual range of parameters.

Thus, for the sake of clarity of the present calculation, we neglect the depolarization field energy in the total free energy in order to establish the net contribution of the other size effects. Although we will make some speculations about the depolarization field, more detailed work on the depolarization field for the inhomogeneous distribution of polarization will be a future objective.

The last term in Eq. (1) is the surface energy with g_{surface} as the surface energy density, and g_{surface} is assumed to be proportional to the square of polarization on the surface S, i.e. $g_{surface} = \frac{1}{2\delta} D P^2$, where δ is the extrapolation length, and D is the gradient energy coefficient [26,38]. The nanowire has left- and right-end surfaces $z = -\frac{h}{2}, \frac{h}{2}$, which are short-circuited or very "remote" in order to be able to neglect the depolarization field, and a sidewall $r = R$ (where R is the radius of the nanowire); thus the surface energy G_s has the form [23]:

$$\begin{aligned} G_S &= \iint_A g_{\text{surface}} dA \\ &= D\left\{ \int_0^R \frac{2\pi r}{\delta_t} dr \left[P^2\left(r, z = -\frac{h}{2}\right) + P^2\left(r, z = \frac{h}{2}\right) \right] \right. \\ &\quad \left. + \int_{-h/2}^{h/2} \frac{2\pi R dz}{\delta_s} P^2(r = R, z) \right\}, \end{aligned} \tag{4}$$

with δ_t the extrapolation length of the left- and right-end surfaces, and δ_s the extrapolation length of the sidewall surface. In order to study the net effect of the radial polarization components, here we omit the surface tension effect, considered in details in Refs. [23,24] for uniaxial polarization P_3.

Hereafter we assume $\delta_t = \delta_s = \delta$, and hence the related boundary condition obtained by the variation of Eq. (4) is $\left(\frac{dP}{dr} + \frac{P}{\delta}\right)\Big|_{r=R} = 0$. Therefore, there must be some inhomogeneous distribution of polarization on the sidewall surface to satisfy the boundary condition, unless δ becomes infinite. However, in this paper, we focus on the strain effects on the phase transition of the nanowire, and thus we continue to neglect the effect on the total energy caused by the inhomogeneity of polarization on the sidewall surface. The approximation makes G_s become:

$$G_S = \frac{2\pi D R^2}{\delta}(P_1^2 + P_2^2 + P_3^2)\left(1 + \frac{h}{R}\right). \tag{5}$$

As $h/R \gg 1$ and $h = V/\pi R^2$ (where V is volume of the nanowire), Eq. (5) is simplified to:

$$G_S = \frac{2DV}{\delta R}(P_1^2 + P_2^2 + P_3^2) = \frac{4DV}{\delta d}(P_1^2 + P_2^2 + P_3^2). \tag{6}$$

Therefore, the total free energy $G(\sigma, T)$ is given by:

$$G(\sigma, T) = \iiint_v [g_{\text{LGD}} + g_{\text{elastic}}] dV + \frac{4DV}{\delta d}(P_1^2 + P_2^2 + P_3^2). \tag{7}$$

3. Results and discussions

We assume that the mismatch between nanowire and substrate induces a misfit strain u_3 along the axis direction, and $u_3 = u_s = \frac{a_s - a_c}{a_c}$, where a_s is the lattice constant of the substrate and a_c is the lattice constant of cubic $BaTiO_3$. For simplicity, the sidewall is considered to be free of surface tension. In the monodomain case, the total strain can be regarded as quasi-homogeneous, and includes the only non-zero component strain u_s [39] Eqs. (8) and (9) give the mathematical expressions of the mechanical boundary condition. Therefore, we have:

$$\frac{\partial G(\sigma, T)}{\partial \sigma_s} = -\iiint_V u_s dV = -u_s V, \tag{8}$$

$$\sigma_1 = \sigma_2 = \sigma_4 = \sigma_5 = \sigma_6 = 0. \tag{9}$$

Substituting Eq. (9) into Eq. (7), the total Gibbs free energy is simplified to:

$$\begin{aligned} G(\sigma, T) = \left[g_{\text{LGD}} - \frac{1}{2} s_{11} \sigma_3^2 - Q_{11} \sigma_3 P_3^2 - Q_{12} \sigma_3 (P_1^2 + P_2^2) \right. \\ \left. + \frac{4D}{\delta d}(P_1^2 + P_2^2 + P_3^2) \right] V, \end{aligned} \tag{10}$$

Combing Eqs. (8) and (10) we can obtain:

$$-s_{11}\sigma_3 - Q_{11}P_3^2 - Q_{12}(P_1^2 + P_{@}^2) = -u_s. \tag{11}$$

The solution of Eq. (11) for σ_3 gives the stress component σ_3 due to the mismatch between the nanowire and substrate, i.e.:

$$\sigma_3 = \frac{u_s - Q_{11}P_3^2 - Q_{12}(P_1^2 + P_2^2)}{s_{11}}. \tag{12}$$

On the other hand, the Helmholtz free energy can be deduced from Legendre transformation:

$$F(u,T) = G(\sigma,T) + \iiint_V (\sigma_1 u_1 + \sigma_2 u_2 + \sigma_3 u_3 + \sigma_4 u_4 + \sigma_5 u_5 + \sigma_6 u_6) dV$$
$$= G(\sigma,T) + \iiint_V \sigma_3 u_3 dV$$
$$= \left[g_{\mathrm{LGD}} - \frac{1}{2} s_{11}\sigma_3^2 - Q_{11}\sigma_3 P_3^2 - Q_{12}\sigma_3(P_1^2+P_2^2) + \frac{4D}{\delta d}(P_1^2+P_2^2+P_3^2) + \sigma_3 u_s \right] V. \quad (13)$$

Substituting Eq. (12) into Eq. (13), the Helmholtz free energy density $f(\vec{P}, u_s, T) = Fu_s, T)/V$ can be expressed as:

$$\begin{aligned} f(\vec{P},u_s,T) = {} & \alpha_1^{\mathrm{NW}}(P_1^2+P_2^2) + \alpha_3^{\mathrm{NW}}P_3^2 + \alpha_{11}^{\mathrm{NW}}(P_1^4+P_2^4) \\ & + \alpha_{33}^{\mathrm{NW}}P_3^4 + \alpha_{13}^{\mathrm{NW}}(P_1^2P_3^2+P_2^2P_3^2) + \alpha_{12}^{\mathrm{NW}}P_1^2P_2^2 \\ & + \alpha_{111}(P_1^6+P_2^6+P_3^6) \\ & + \alpha_{112}\left[P_1^4(P_2^2+P_3^2) + P_2^4(P_1^2+P_3^2) + P_3^4(P_1^2+P_2^2)\right] \\ & + \alpha_{1123}P_1^2P_2^2P_3^2 + \alpha_{1111}(P_1^8+P_2^8+P_3^8) \\ & + \alpha_{1122}(P_1^4P_2^4+P_1^4P_3^4+P_2^4P_3^4) \\ & + \alpha_{1112}\left[P_1^6(P_2^2+P_3^2) + P_2^6(P_1^2+P_3^2) + P_3^6(P_1^2+P_2^2)\right] \\ & + \alpha_{1123}(P_1^4P_2^2P_3^2 + P_1^2P_2^4P_3^2 + P_1^2P_2^2P_3^4) \end{aligned} \quad (14)$$

where α_1^{NW}, α_3^{NW}, $\alpha_{11}^{\mathrm{NW}}$, $\alpha_{33}^{\mathrm{NW}}$, $\alpha_{12}^{\mathrm{NW}}$, $\alpha_{13}^{\mathrm{NW}}$ are functions of original coefficients at constant stress, i.e.:

$$\alpha_1^{\mathrm{NW}} = \alpha_1 + \frac{4D}{\delta d} - \frac{u_s Q_{12}}{s_{11}}, \quad (15)$$
$$\alpha_3^{\mathrm{NW}} = \alpha_1 + \frac{4D}{\delta d} - \frac{u_s Q_{11}}{s_{11}}, \quad (16)$$
$$\alpha_{11}^{\mathrm{NW}} = \alpha_{11} + \frac{Q_{12}^2}{2s_{11}}, \quad (17)$$
$$\alpha_{33}^{\mathrm{NW}} = \alpha_{11} + \frac{Q_{11}^2}{2s_{11}}, \quad (18)$$
$$\alpha_{12}^{\mathrm{NW}} = \alpha_{12} + \frac{Q_{12}^2}{2s_{11}}, \quad (19)$$
$$\alpha_{13}^{\mathrm{NW}} = \alpha_{12} + \frac{Q_{11}^2 Q_{12}}{2s_{11}}. \quad (20)$$

Therefore, the Helmholtz free energy density is a function of the polarization, temperature, misfit strain and diameter of the nanowires. In the modified Landau potential coefficients from Eqs. (15)–(20), the values of the gradient energy coefficient D and the extrapolation length δ are typically not known. D is connected to the correlation length ξ, $D = \xi^2|A(T - T_{C\infty}|$, where A is determined by α_1, and $T_{C\infty}$ is the Curie temperature of the bulk crystal [26]. The extrapolation length δ describes the polarization difference between the surface and bulk. It depends not only on the different interaction constants at the surface and in the bulk, but also on the coordination number at the surface. For pseudospins forming a simple cubic lattice with a lattice constant a_0, if the interaction constant is J_s for pseudospins on the surface and is J elsewhere, then δ can be expressed as $\delta = a_0 J/(5J - 4J_s)$ [26,40].

The material parameters used for calculation in this work are presented as follows (from Refs. [25,41,28,42,21,43]):

$\alpha_1 = 5.0 \times 10^5 \times T_s\left[\mathrm{Coth}\left(\frac{T_s}{T}\right) - \mathrm{Coth}\left(\frac{T_s}{390}\right)\right]\mathrm{Vm\,C^{-1}}, T_s = 160\ \mathrm{K}$
$\alpha_{11} = -1.154 \times 10^8\ \mathrm{Vm^5\,C^{-3}}, \alpha_{12} = 6.530 \times 10^8\ \mathrm{Vm^5\,C^{-3}}, \alpha_{111} = -2.103 \times 10^9\ \mathrm{Vm^9\,C^{-5}},$
$\alpha_{112} = 4.091 \times 10^9\ \mathrm{Vm^9\,C^{-5}}, \alpha_{123} = -6.688 \times 10^9\ \mathrm{Vm^9\,C^{-5}}, \alpha_{1111} = 7.590 \times 10^{10}\ \mathrm{Vm^{13}\,C^{-7}},$
$\alpha_{1112} = -2.193 \times 10^{10}\ \mathrm{Vm^{13}\,C^{-7}}, \alpha_{1122} = -2.221 \times 10^{10}\ \mathrm{Vm^{13}\,C^{-7}}$
$\alpha_{1123} = -2.416 \times 10^{10}\ \mathrm{Vm^{13}\,C^{-7}}, s_{11} = 9.07 \times 10^{12}\ \mathrm{m^2/N}, S_{12} = -3.186 \times 10^{-12}\ \mathrm{m^2/N},$
$S_{44} = 1.22 \times 10^{-12}\ \mathrm{m^2/N}, Q_{11} = 0.11\ \mathrm{m^4/C^2}, Q_{12} = 0.045\ \mathrm{m^4/C^2}, Q_{44} = 0.029\ \mathrm{m^4/C^2},$
$D = 0.9 \times 10^{-9}\ \mathrm{m^3/F}.$

The extrapolation length δ can be negative or positive. δ can be fitted to the experimentally measured Curie temperature of a particle with given size [38]. In addition, it can be obtained by estimating the surface relaxation length [43]. However, δ can be very different if fitted to different experimental measurements. For instance, Wang et al. obtained a value of 43 nm for δ by fitting it to earlier experimental data of $BaTiO_3$ particles [26,38], and Ishikawa et al. estimated a value of 88 nm for δ from their experimental measurement of $BaTiO_3$ particles [43]. As the coordination number at the surface will be different for different structures, δ could not be the same for $BaTiO_3$ nanowires and particles. Therefore, we refitted δ to Spanier et al.'s experimental data for $BaTiO_3$ nanowires which have a Curie temperature of about 300 K at a diameter of 3 nm [14]. The refitted δ is 29 nm, i.e. smaller than the previous two results obtained from nanoparticles.

Based on the above parameters and analysis, curves for the Curie temperature T_c of $BaTiO_3$ nanowires with different diameter d are obtained and are shown in Fig. 2. It is observed that the size does not have a dramatic effect on the Curie temperature when the diameter is above 20 nm, which is similar as Hong et al.'s conclusion [21]. As expected, with the increase in size, the Curie temperature becomes closer to the bulk case, following $1/d$ scaling. The calculated Curie temperature vs. diameter curve agrees

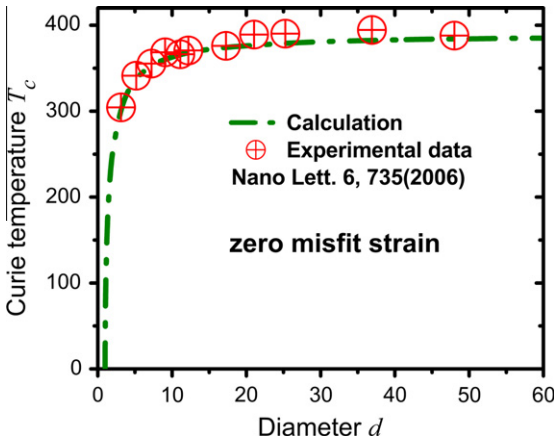

Fig. 2. Curie temperature T_C of $BaTiO_3$ nanowire with different diameters d calculated at zero misfit strain, and compared with existing experimental data.

well with existing experimental measurement. Based on Fig. 1, the critical diameter at which the ferroelectricity disappears is around 1.0 nm, compared with 0.8 nm extrapolated from Spanier et al.'s experimental data and 1.2 nm from Hong et al.'s calculation [21,14].

For a paraelectric $BaTiO_3$ material with symmetry group $m3m$, six ferroelectric phases are possible with polarization $(P_1, 0, 0)$, $(P_1, P_1, 0)$, (P_1, P_1, P_1), $(P_1, P_2, 0)$, (P_1, P_1, P_2) or (P_1, P_2, P_3) and their equivalent counterparts. For a bulk crystal that is stress-free or subjected to hydrostatic pressure, only three ferroelectric phases are stable from both experimental observation and theoretical models: tetragonal with polarization of $(P_1, 0, 0)$, orthorhombic phase $(P_1, P_1, 0)$ and rhombohedral phase (P_1, P_1, P_1) [25,41,44,45]. For thin films epitaxially grown on different substrates with clamped in-plane boundary conditions and stress-free out-of-plane boundary conditions, four ferroelectric phases are stable according to previous phenomenological thermodynamic calculations: tetragonal phase with polarization of $(0, 0, P_3)$, orthorhombic $(P_1, P_1, 0)$, monoclinic $(P_1, 0, P_2)$ and distorted rhombohedral (P_1, P_1, P_2) [27]. Fig. 3 shows the strain–temperature phase diagrams, which are constructed by minimizing the Helmholtz free energy density $f(\vec{P}, u_s, T)$ for $BaTiO_3$ nanowires at a given diameter, where the modified Landau potential was used for the calculation [25]. It can be seen from Fig. 3a that six possible ferroelectric phases can be stable at different temperature and misfit strain conditions. Therefore, the distortion of the lattice structure due to the misfit between the substrate and the thin film, or nanowire, can induce extra ferroelectric phases compared with the stress-free bulk case. Fig. 3b shows that the decrease of the diameter depresses the area of the ferroelectric phases on the phase diagrams. In other words, all the transition temperatures, including transition temperatures from paraelectric phase to ferroelectric phase and from one ferroelectric phase to another ferroelectric phase, decrease as the diameter of the $BaTiO_3$ nanowire decreases. At low temperatures, the boundary lines in the phase diagrams exhibit an exponential decrease rather than a linear decrease due to the low-temperature quantum effects expressed by the Landau potential coefficient α_1. The Curie temperature is increased linearly by the tensile or compressive misfit strain, and is determined by the electrostrictive coefficients and elastic compliance tensor. A further consequence is that the polarization will rotate close to the axial direction of the nanowire with misfit strain changing from compressive to tensile. In other words, the polarization component P_3 will be increased by the tensile strain and decreased by the compressive strain, which is very consistent with the MD simulation of Zhang et al. [20].

Fig. 4 compares the misfit strain and temperature phase diagrams for $BaTiO_3$ nanowires with a diameter of 200 nm calculated from previously published eighth-order Landau potentials of Li et al. and Wang et al. and the modified potential [25,45,46]. It can be seen that all three Landau potentials give similar misfit strain and

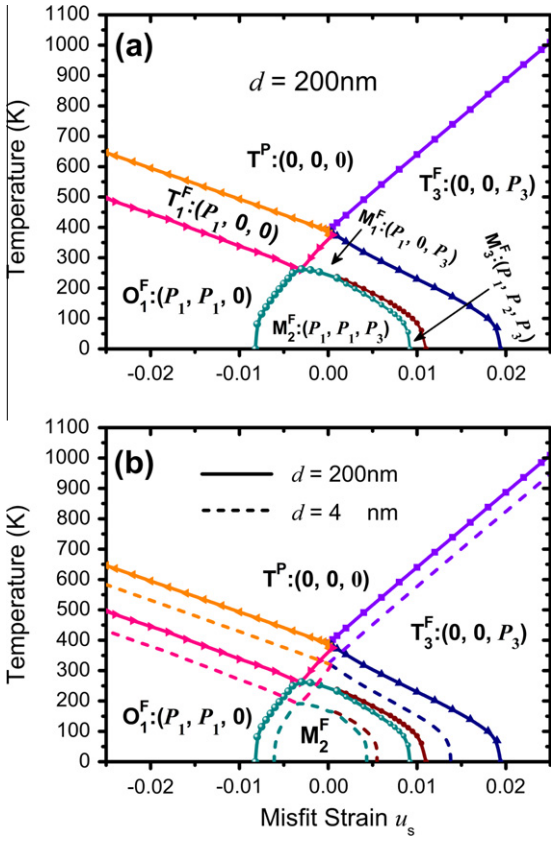

Fig. 3. Temperature–misfit strain phase diagrams of $BaTiO_3$ nanowires. (a) Phase diagram for 200 nm diameter nanowires includes six ferroelectric phases having polarization vectors of $\vec{P} = (\pm P_1, 0, 0)/(0, \pm P_2, 0$ inT_1^F, $\vec{P} = (0, 0, \pm P_3)$ in T_3^F, $\vec{P} = (\pm P_1, \pm P_1, 0)/(\pm P_1, \mp P_1, 0)$ in O_1^F, $\vec{P} = (\pm P_1, 0, \pm P_3)/(\pm P_1, 0, \mp P_3)/(0, \pm P_2, \pm P_3)/(0, \pm P_2, \mp P_3)$ in M_1^F, $\vec{P} = (\pm P_1, \pm P_1, \pm P_3)/(\pm P_1, \mp P_1, \mp P_3)/(\pm P_1, \pm P_1, \mp P_3)/(\pm P_1, \mp P_1, \mp P_3)$ in M_2^F, $\vec{P} = (\pm P_1, \pm P_2, \pm_3)/(\pm P_1, \mp P_2, \pm P_3)/(\pm P_1, \pm P_2, \mp P_3)/ (\pm P_1, \mp P_2, \mp P_3)$ in M_3^F. (b) Comparison between two diagrams of nanowires with diameters of 200 nm (solid line) and 4 nm (short-dashed line).

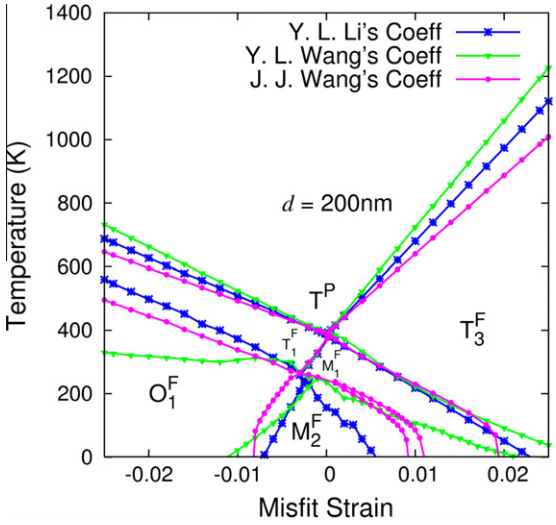

Fig. 4. Temperature–misfit strain phase diagrams of 200 nm diameter $BaTiO_3$ nanowires calculated from different Landau potentials. The definitions of the phases are the same as in Fig. 3.

temperature phase diagrams, including five ferroelectric areas with polarization, $\overrightarrow{P} = (P_1, 0, 0)$ in T_1^F, $\overrightarrow{P} = (0, 0, P_3)$ in T_3^F, $\overrightarrow{P} = (P_1, P_1, 0)$ in O_1^F, $\overrightarrow{P} = (P_1, 0, P_3)$ in M_1^F, $\overrightarrow{P} = (P_1, P_1, P_3)$ in M_2^F, and one paraelectric area with polarization, $\overrightarrow{P} = (0, 0, 0)$ in T^P. However, there are indeed some obvious differences between the three phase diagrams. For example, the slopes for the boundaries of the paraelectric phases and ferroelectric phases are different, indicating that the rates of increase for the Curie temperatures with misfit strains are different. The sharpest is from Wang et al.'s coefficients, the second is from Li et al.'s coefficients, and the smoothest is from the newly modified coefficients. Another obvious difference comes from the ferroelectric phase boundaries at low temperature. Only the newly modified Landau potentials exhibit an exponential trend as the quantum effects are considered, whereas the other two sets of coefficients show approximately linear trends. Additionally, the new modified Landau coefficients also give another ferroelectric monoclinic phase with polarization $\overrightarrow{P} = (P_1, P_2, P_3)$ in M_3^F which is not obtained from the other two sets of Landau coefficients. This new phase is stable in a very narrow area at low temperature, and we speculate that it may be due to the quantum effect term in the first-order Landau coefficient. However, the rationale for the appearance of the new ferroelectric phase of M_3^F needs experimental confirmation and symmetry analysis, and here we just report the calculation result.

Although the depolarization field effect on the total free energy was not considered for simplicity, some speculations about the depolarization field are still necessary. Eq. (A6) in Appendix A can be used to estimate the magnitude of the depolarization field induced by screening the charges coming from the ambient environment. The introduction of the depolarization field energy to the total free energy must change the modified Landau potential coefficient from α_1^{NW} to α_1^{NW*} by $\alpha_1^{NW*} = \alpha_1^{NW} + \frac{\eta}{\varepsilon_0\varepsilon_b}$. The phase boundaries in Fig. 3 will accordingly be altered, but these changes are slight up to $\frac{\eta}{\varepsilon_0\varepsilon_b}$. Taking the Curie temperature as an example, if the depolarization field effect leads to an value of 10^6 Vm C^{-1} for $\frac{\eta}{\varepsilon_0\varepsilon_b}$, the Curie temperature will decrease by 2 K for a 3 nm diameter nanowire, compared with the calculation without the depolarization field. On the other hand, the decrease in the Curie temperature caused by the depolarization field effect weakens with an increase in diameter.

4. Summary

We used a modified Landau phenomenology to describe the phase transition behavior due to the effects of strain and size for $BaTiO_3$ nanowires taking into consideration three components of polarization. We demonstrated that the Curie temperature is essentially governed by the mismatch strain between the nanowire and substrate. The completely constructed temperature and strain phase diagram shows six possible ferroelectric phases. For $BaTiO_3$ nanowires with zero misfit strain the critical diameter, below which the ferroelectric phases totally disappear, is around 1.0 nm. The calculated variation in Curie temperature vs. diameter agrees well with existing experimental measurements.

Acknowledgements

This work was partially sponsored by the Project-Based Personnel Exchange Program by the China Scholarship Council and American Academic Exchange Service ([2008] 3012) and partially funded by NSF under DMR0908718, DMR-0820404 and DMR-1006541. The computations were performed using the Cyberstar cluster at the Pennsylvania State University, funded by the National Science Foundation through Grant OCI-0821527. A.N.M. and E.E.A.'s research was sponsored in part by the Ukraine State Committee on Science, Innovation and Information (UU30/004) and National Science Foundation (DMR-0908718).

Appendix A

We suppose that the depolarization field is created by the polarization components perpendicular to the symmetry axis of the wire and depends only on the distance to this axis, i.e. $P_{x,y}(\rho)$. Let us introduce the cylindrical coordinate system (ρ, ϑ, z) with polar radius ρ, angle ϑ and z axis along the symmetry axis.

A.1. Extrinsic size effect contribution via the depolarization field due to the incomplete external screening. Polarization is homogeneous inside the nanoparticle

Let us substitute the real shape of a given nanoparticle by an equivalent nanowire of radius R. First, we calculate the depolarization field for the simplest case of a dielectrically isotropic core, shell and ambient materials. We consider a zero external field, since equations of electrostatics are linear and the corresponding solution for the cylinder with concentric shell in the homogeneous external field could be added to the solution found below [47].

The equations of state relating displacement **D**, electric field **E** and polarization **P** are:

$$\mathbf{D}_i \approx \mathbf{P} + \varepsilon_0\varepsilon_b\mathbf{E}_i, \quad \mathbf{D}_s = \varepsilon_0\varepsilon_s\mathbf{E}_s, \quad \mathbf{D}_e = \varepsilon_0\varepsilon_e\mathbf{E}_e. \tag{A1}$$

Here we used the so-called linearized model of FNW core polarization and introduced its isotropic dielectric permittivity $\varepsilon_{11} = \varepsilon_{33} = \varepsilon_b$, where ε_b is called the background or reference state permittivity [34]. The external screening layer "s" has permittivity ε_s; the ambient medium "e" has permittivity ε_e.

Hereinafter we introduce the potential of electric field $\mathbf{E} = -\nabla\varphi(\mathbf{r})$. In cylindrical coordinates $\mathbf{r} = \{\rho, \vartheta, z\}$ the potential inside each region i, s, e acquires the form:

$$\varphi(\rho,\vartheta)=\begin{cases}\varphi_{\rm i}(\rho,\vartheta), & 0\leqslant\rho<R,\\ \varphi_{\rm s}(\rho,\vartheta), & R\leqslant\rho<R_o,\\ \varphi_{\rm e}(\rho,\vartheta), & \rho\geqslant R_o.\end{cases}\tag{A2}$$

R is the nanowire radius, and R_o is the shell radius. The Maxwell equation $\mathrm{div}\mathbf{D}=0$ should be supplied with boundary conditions:

$$(\varphi_{\rm i}-\varphi_{\rm s})|_{\rho=R}=0,\quad (\mathbf{D}_{\rm s}-\mathbf{D}_{\rm i})\mathbf{e}_\rho=(-\varepsilon_0\varepsilon_{\rm s}\frac{\partial\varphi_{\rm s}}{\partial\rho}+\varepsilon_0\varepsilon_{\rm b}\frac{\partial\varphi_{\rm i}}{\partial\rho}-P_x\cos\vartheta)\Big|_{\rho=R}=0,$$
$$(\varphi_{\rm s}-\varphi_{\rm e})|_{\rho=R_o}=0,\quad (\mathbf{D}_{\rm e}-\mathbf{D}_{\rm s})\mathbf{e}_\rho=\varepsilon_0(-\varepsilon_{\rm e}\frac{\partial\varphi_{\rm e}}{\partial\rho}+\varepsilon_{\rm s}\frac{\partial\varphi_{\rm s}}{\partial\rho})\Big|_{\rho=R_o}=0,$$
$$\varphi_{\rm i}|_{\rho=0}<\infty,\quad \varphi_{\rm e}|_{\rho\to\infty}=0\tag{A3}$$

Here $\mathbf{e}_\rho$ is the outer normal to the cylindrical surface.

As the first step we suppose that the polarization inside the wire is homogeneous. The electrostatic potential inside the particle and screening layer satisfies the Laplace equation $\Delta\varphi=0$, while the media outside the particle may be semiconducting, its potential should satisfy the equation $\Delta\varphi_{\rm e}-\varphi_{\rm e}/l_{\rm d}^2=0$ according to the Debye approximation with screening length $l_{\rm d}$.

The general solution of the Laplace equation $\Delta\varphi=0$, depending only on radius ρ and polar angle ϑ is:

$$\varphi(\rho,\vartheta)=a_0+b_0\ln(\rho)+\sum_{n=1}^{\infty}(a_n\rho^n+\frac{b_n}{\rho^n})\cos(n\vartheta+\vartheta_n)\tag{A4}$$

where a_n and b_n are constants. One should leave in Eq. (A4) the terms with $n=1$; only. Thus we derived the solution as [48]:

$$\varphi_{\rm i}(\rho,\vartheta)=a\rho\cos\vartheta,\quad 0\leqslant\rho<R.\tag{A5a}$$

Potential (18a) corresponds to a homogeneous field equal to −a:

$$\varphi_{\rm s}(\rho,\vartheta)=(c\rho+\frac{b}{\rho})\cos\vartheta,\quad R\leqslant\rho<R_o,\tag{A5b}$$
$$\varphi_{\rm e}(\rho,\vartheta)=(d\ K_1(\rho/l_{\rm d})+fI_1(\rho/l_{\rm d}))\cos\vartheta,\quad \rho\geqslant R_o.\tag{A5c}$$

Here I_1 and K_1 are the modified Bessel function of the first and second kind, respectively.

Boundary conditions (A3) give the system of linear equations for constants a, b, c, d, f. The electric field inside the ferroelectric wire ($r<R$) is expressed via the effective depolarization factor η as follows:

$$E_1=-\frac{P_1}{\varepsilon_0\varepsilon_{\rm b}}\eta,\quad \rho<R.\tag{A6}$$

The effective depolarization factor η essentially depends on the surroundings, namely:

(a) For the ferroelectric wire in a semiconductor matrix the factor η equals:

$$\eta=\frac{l_dK_1(R/l_d)\varepsilon_b}{(RK_0(R/l_d)+l_dK_1(R/l_d))\varepsilon_e+l_dK_1(R/l_d)\varepsilon_b}.\tag{A7a}$$

It is noteworthy that $\eta\approx\frac{\varepsilon_{\rm b}}{\varepsilon_{\rm e}}\frac{l_{\rm d}}{R}$, for $R>>l_{\rm d}$.

(b) For the "ferroelectric wire/dielectric shell /dielectric matrix" the factor η is:

$$\eta=\frac{(R_o^2(\varepsilon_{\rm s}+\varepsilon_{\rm e})-R^2(\varepsilon_{\rm e}-\varepsilon_{\rm s}))\varepsilon_{\rm b}}{R_o^2(\varepsilon_{\rm b}+\varepsilon_{\rm s})(\varepsilon_{\rm s}+\varepsilon_{\rm e})+R^2(\varepsilon_{\rm s}-\varepsilon_{\rm b})(\varepsilon_{\rm e}-\varepsilon_{\rm s})}\tag{A7b}$$

In the limiting case $\varepsilon_{\rm e}\to\infty$ corresponding to the system "ferroelectric wire/dielectric shell/conducting matrix" one has the following expression $\eta=\frac{(R_o^2-R^2)\varepsilon_{\rm b}}{R_o^2(\varepsilon_{\rm b}+\varepsilon_{\rm s})+R^2(\varepsilon_{\rm s}-\varepsilon_{\rm b})}$ and $\eta\approx\frac{\varepsilon_{\rm b}}{\varepsilon_{\rm s}}\frac{R_o-R}{R_o}$, for $R>>R_o-R$.

(c) For the "ferroelectric wire/dielectric shell/dielectric matrix" the factor η is:

$$\eta=\frac{(R_o^2(\varepsilon_{\rm s}+\varepsilon_{\rm e})-R^2(\varepsilon_{\rm e}-\varepsilon_{\rm s}))\varepsilon_{\rm b}}{R_o^2(\varepsilon_{\rm b}+\varepsilon_{\rm s})(\varepsilon_{\rm s}+\varepsilon_{\rm e})+R^2(\varepsilon_{\rm s}-\varepsilon_{\rm b})(\varepsilon_{\rm e}-\varepsilon_{\rm s})}\tag{A7c}$$

In the limiting case $\varepsilon_{\rm e}\to\infty$, corresponding to the system "ferroelectric wire/dielectric shell/screening outside", one has the following expression: $\eta=\frac{(R_o^2-R^2)\varepsilon_{\rm b}}{R_o^2(\varepsilon_{\rm b}+\varepsilon_{\rm s})+R^2(\varepsilon_{\rm s}-\varepsilon_{\rm b})}$ and $\eta\approx\frac{\varepsilon_{\rm b}}{\varepsilon_{\rm s}}\frac{R_o-R}{R_o}$, for $R>>R_o-R$.

Depolarization effects can be neglected under the condition of negligibly small depolarization energy in comparison with the LGD energy: $|\alpha_1^{\rm NW}|P_1^2>>\frac{1}{\varepsilon_0\varepsilon_{\rm b}}P_1^2|\eta|$, i.e. when the strong inequality $|\eta|<<\varepsilon_0\varepsilon_{\rm b}|\alpha_1^{\rm NW}|$ is valid. More roughly, the inequality $\varepsilon_0\varepsilon_{\rm b}|\alpha_1|/|\eta|>>1$ needs to be satisfied for the depolarization effect to be negligibly small.

In Fig. A1 we compare the reduced depolarization factor from Eq. (A7b) in the limit $\varepsilon_{\rm e}\to\infty$, i.e. $\frac{\eta(\varepsilon_{\rm e}\to\infty)}{\varepsilon_{\rm b}}=\frac{(R_o^2-R^2)}{R_o^2(\varepsilon_{\rm b}+\varepsilon_{\rm s})+R^2(\varepsilon_{\rm s}-\varepsilon_{\rm b})}$ with $\varepsilon_0|\alpha_1|$ at fixed shell permittivity $\varepsilon_{\rm s}$, dielectric shell thickness $\delta R=R_o-R$, for various temperatures and wire radii. Typically $\delta R\leqslant 1$ nm, since there is a very small distance between bound charges (i.e. polarization charges) and free screening charges [37].

It can be seen from Fig. A1c and d that the contribution of the depolarization field to the total energy is negligibly small (i.e. $|\varepsilon_0\varepsilon_b\alpha_1(T)/\eta(R)|>10$) in the actual range of parameters, e.g. $R_o>10$ nm and $T<300$ K (or $T>500$ K) at $\varepsilon_{\rm s}\sim\sqrt{\varepsilon_{11}^{BTO}\varepsilon_{33}^{BTO}}\sim10^3$ and $\delta R=0.5$ nm. These results prove that η can be tuned as small as necessary by high $\varepsilon_{\rm e}$, $\varepsilon_{\rm s}$, etc., and gives us some grounds not to include the depolarization field energy in the total free energy in order to establish the net contribution of other size effects.

A.2. Intrinsic size effect contribution via the depolarization field due to the incomplete external screening and inhomogeneous polarization inside the nanowire

As the second step let us consider the case of inhomogeneous polarization inside the wire, supposing only a radial dependence, $P_x(\rho)$. Below we show that it is not rigorous, but in some cases this could be the first approximation.

A.2.1. The ideally screening ambient media

First, we consider the wire inside the ideally screening ambient media ($l_d \to 0$) without a dielectric shell. It is obvious that the solution of more complicated problems could be constructed by an appropriate combination of simpler solutions.

The electrostatic potential inside the wire satisfies Poisson equation. For the case of $\mathbf{P} = (P_1(\rho), 0, 0)$ this reduces to:

$$\Delta\varphi = \frac{\cos\vartheta}{\varepsilon_0\varepsilon_b}\frac{\partial P_x(\rho)}{\partial\rho}. \tag{A8}$$

Boundary conditions are:

$$\varphi|_{\rho=0} < \infty, \quad \varphi|_{\rho=R} = 0. \tag{A9}$$

It is natural to look for the solution of (A9) in the form of a Fourier series $\varphi(\rho,\vartheta) = \sum_{n=0}^{\infty}(f_n(\rho)\cos n\vartheta + g_n(\rho)\sin n\vartheta)$. Using the orthogonality of Fourier harmonics, one can see that only the term with $n = 1$ will be sufficient. Thus, introducing the Ansatz $\varphi(\rho,\vartheta) = \psi(\rho)\cos\vartheta$, we obtain:

$$\frac{\partial^2\psi(\rho)}{\partial\rho^2} + \frac{1}{\rho}\frac{\partial\psi(\rho)}{\partial\rho} - \frac{1}{\rho^2}\psi(r) = \frac{1}{\varepsilon_0\varepsilon_b}\frac{\partial P_x(\rho)}{\partial\rho}. \tag{A10}$$

The solution of (A10) can be found in the form:

$$\psi(\rho) = \frac{1}{\varepsilon_0\varepsilon_b}\left(\frac{1}{\rho}\int_0^{\rho} P_x(\tilde{r})\tilde{r}d\tilde{r} - \frac{\rho}{R^2}\int_0^{R} P_x(\tilde{r})\tilde{r}d\tilde{r}\right). \tag{A11}$$

Now we can find the electric field $\mathbf{E} = -\nabla(\psi(\rho)\cos\vartheta)$. The x-component is:

$$\begin{aligned} E_x(\rho,\vartheta) &= -\cos\vartheta\frac{\partial(\psi(\rho)\cos\vartheta)}{\partial\rho} + \frac{\sin\vartheta}{\rho} \\ &\quad\times\frac{\partial(\psi(\rho)\cos\vartheta)}{\partial\theta} \\ &= -\cos^2\vartheta\frac{\partial(\psi(\rho))}{\partial\rho} - \sin^2\vartheta\frac{\psi(\rho)}{\rho} \end{aligned} \tag{A12}$$

It can be seen that the x-component could be independent of ϑ in the very specific case $\psi(\rho) \sim \rho$ only (which also means that $E_x = const$). That is why the supposition $P_x(\rho)$ is not rigorous. However, the evident expression for E_x obtained from Eqs. (A11) and (A12) could be written for a given distribution of $P_x(\rho)$ as:

$$\begin{aligned} E_x(\rho,\vartheta) &= \frac{1}{\varepsilon_0\varepsilon_b}\left(\frac{1}{R^2}\int_0^{R} P_x(\tilde{r})\tilde{r}d\tilde{r} - \cos^2\vartheta P_x(\rho)\right. \\ &\quad\left.+\frac{\cos^2\vartheta - \sin^2\vartheta}{\rho^2}\int_0^{\rho} P_x(\tilde{r})\tilde{r}d\tilde{r}\right) \\ &= \frac{1}{\varepsilon_0\varepsilon_b}\left(\frac{1}{R^2}\int_0^{R} P_x(\tilde{r})\tilde{r}d\tilde{r} - \frac{1}{2}P_x(\rho) - \frac{\cos 2\vartheta}{2\rho^2}\times\int_0^{\rho}\frac{\partial P_x(\tilde{r})}{\partial\tilde{r}}\tilde{r}^2 d\tilde{r}\right) \end{aligned} \tag{A13}$$

It can be seen that the first two terms could be reduced to the form proposed by us earlier on the basis of the variation method: $E_1 \approx (\langle P_1(\rho)\rangle - P_1(\rho))/(2\varepsilon_0\varepsilon_b)$ [49]; these terms are independent of angle ϑ. The last term in

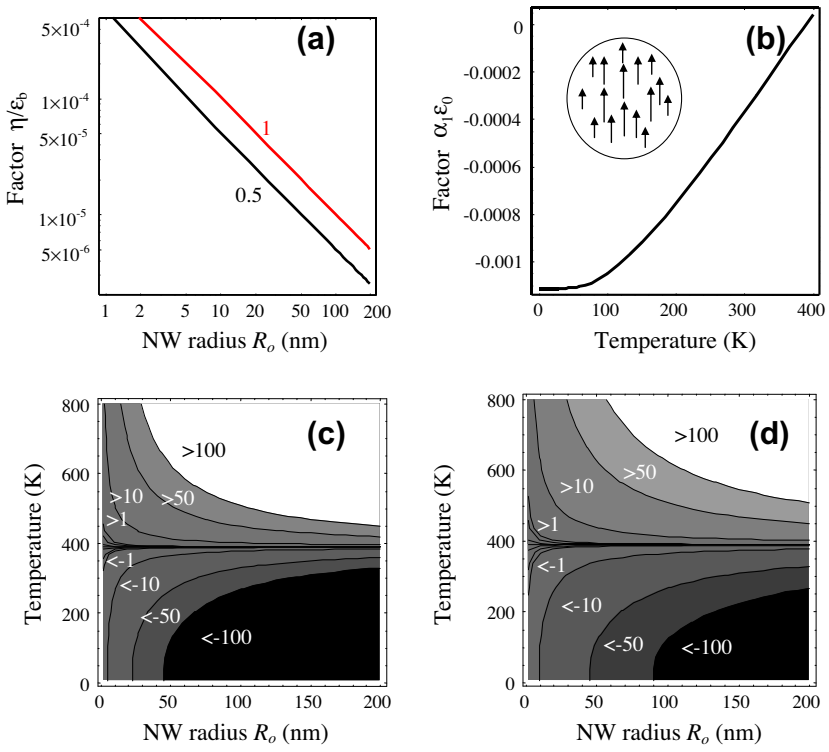

Fig. A1. (a) Depolarization factor $\eta(\varepsilon_e \to \infty)/\varepsilon_b$ vs. nanowire outer radius R_0 calculated for dielectric shell thickness $\delta R = 0.5$ and 1 nm (figures near the curves). (b) The temperature dependence of coefficient $\varepsilon_0\alpha_1$. Inset shows the polarization direction in the nanowire cross-section. (c and d) Contour maps of the ratio $\varepsilon_0\varepsilon_b\alpha_1(T)/\eta(R)$ calculated for dielectric shell thickness $\delta R = 0.5$ nm (c) and 1 nm (c). Contour lines correspond to the values $\{-100,-50,-10,-1,-0.5,-0.1,0,0.1,0.5,1,10,50,100\}$. Other parameters: $\varepsilon_b = 50$, nanowire shell permittivity $\varepsilon_s = 1000$, $\alpha_1(T) = 5.0\times10^5\times T_s\left[\mathrm{Coth}\left(\frac{T_s}{T}\right) - \mathrm{Coth}\left(\frac{T_s}{390}\right)\right]\mathrm{Vm\,C^{-1}}$, $T_s = 160$ K, dielectric constant $\varepsilon_0 = 8.85\times10^{-12}$ F m^{-1}.

Eq. (A13) is proportional to cos 2ϑ and corresponds to the inhomogeneous divergent field. However, it has an impact only on the regions of the particle outside the range where the polarization changes rapidly. For example, if one has a particle with almost constant polarization throughout the wire except near a thin surface layer, $\partial P_3(\rho)/\partial\rho \approx 0$ at $0 < \rho < R - \delta R$, and surface layer with gradient polarization, $\rho\partial P_3(\rho)/\partial\rho \sim P_3(\rho)$ at $R - \delta R < \rho < R$, then the divergent term in (A13) could be of order of the first two terms only in the surface layer $R - \delta R < \rho < R$.

A.2.2. The semiconducting ambient media

For the case of a FNW inside a semiconducting ambient media with a screening length l_d, let us look for the solution in the form (compare with Eq. (A5c)):

$$\psi_i(\rho) = \frac{1}{\varepsilon_0\varepsilon_b}\left(\frac{1}{\rho}\int_0^\rho P_x(\tilde{r})\tilde{r}d\tilde{r} - \frac{\rho}{R^2}\int_0^R P_x(\tilde{r})\tilde{r}d\tilde{r}\right) - E_i\rho, \quad \rho < R, \tag{A14a}$$

$$\psi_e(\rho) = -RE_eK_1\left(\frac{\rho}{l_d}\right), \quad \rho \geqslant R. \tag{A14b}$$

Using the conditions:

$$(\psi_i - \psi_e)|_{\rho=R} = 0, \qquad \left(-\varepsilon_0\varepsilon_e\frac{\partial\psi_e}{\partial\rho} + \varepsilon_0\varepsilon_b\frac{\partial\psi_i}{\partial\rho} - P_x\right)\Big|_{\rho=R} = 0,$$
$$\psi_i|_{\rho=0} < \infty, \quad \psi_e|_{\rho\to\infty} = 0 \tag{A15}$$

it is possible to find the constants E_i and E_e and then to write the solution for the potential inside the nanoparticle in the form:

$$\psi_i(\rho) = \frac{1}{\varepsilon_0\varepsilon_b}\left(\frac{1}{\rho}\int_0^\rho P_x(\tilde{r})\tilde{r}d\tilde{r} - \frac{\rho}{R^2}\int_0^R P_x(\tilde{r})\tilde{r}d\tilde{r}\right) + \frac{\rho}{\varepsilon_0}\frac{2}{R^2}\int_0^R P_x(\tilde{r})\tilde{r}d\tilde{r}\frac{l_dK_1(R/l_d)}{(RK_0(R/l_d) + l_dK_1(R/l_d))\varepsilon_e + l_dK_1(R/l_d)\varepsilon_b}, \quad \rho < R \tag{A16}$$

The electric field x-component inside the nanowire is

$$E_x = \frac{1}{\varepsilon_0\varepsilon_b}\left(\frac{1}{R^2}\int_0^R P_x(\tilde{r})\tilde{r}d\tilde{r} - \frac{1}{2}P_x(\rho) - \frac{\cos 2\vartheta}{2\rho^2}\int_0^\rho \frac{\partial P_x(\tilde{r})}{\partial\tilde{r}}\tilde{r}^2d\tilde{r}\right) - \frac{1}{\varepsilon_0}\frac{2}{R^2}\int_0^R P_x(\tilde{r})\tilde{r}d\tilde{r}\frac{l_dK_1(R/l_d)}{(RK_0(R/l_d) + l_dK_1(R/l_d))\varepsilon_e + l_dK_1(R/l_d)\varepsilon_b} \tag{A17}$$

The last term in Eq. (A17) is related to the non-ideal screening either due to the dead layer or to the finite screening length (compare with Eq. (A7a)).

An approximation is valid:

$$\frac{(RK_0(R/l_d) + l_dK_1(R/l_d))}{l_dK_1(R/l_d)} \approx \sqrt{\frac{R^2}{l_d^2} + \frac{R}{l_d} + 1}. \tag{A18}$$

Neglecting any stray field, one can obtain the following from Eqs. (A17) and (A18):

$$E_x \approx \frac{1}{\varepsilon_0\varepsilon_b}\left(\frac{1}{R^2}\int_0^R P_x(\tilde{r})\tilde{r}d\tilde{r} - \frac{1}{2}P_x(\rho)\right) - \frac{2}{R^2} \times \int_0^R P_x(\tilde{r})\tilde{r}d\tilde{r}\frac{l_d}{\varepsilon_0\left(\varepsilon_e\sqrt{R^2 + l_dR + l_d^2} + \varepsilon_b l_d\right)} \tag{A19}$$

References

[1] Lines ME, Glass AM. Oxford: Clarendon Press; 1979.
[2] Scott JF, Dearaujo CAP. Science 1989;246:1400.
[3] Scott JF. Science 2007;315:954.
[4] Evans PR, Zhu XH, Baxter P, McMillen M, McPhillips J, Morrison FD, et al. Nano Lett 2007;7:1134.
[5] Naumov II, Bellaiche L, Fu HX. Nature 2004;432:737.
[6] Alexe M, Hesse D, Schmidt V, Senz S, Fan HJ, Zacharias M, et al. Appl Phys Lett 2006;89:172907.
[7] Luo Y, Szafraniak I, Zakharov ND, Nagarajan V, Steinhart M, Wehrspohn RB, et al. Appl Phys Lett 2003;83:440.
[8] Mao YB, Banerjee S, Wong SS. J Am Chem Soc 2003;125:15718.
[9] Urban JJ, Yun WS, Gu Q, Park H. J Am Chem Soc 2002;124:1186.
[10] Liu JF, Li XL, Li YD. J Nanosci Nanotechnol 2002;2:617.
[11] Wang ZY, Suryavanshi AP, Yu MF. Appl Phys Lett 2006;89:082903.
[12] Yun WS, Urban JJ, Gu Q, Park H. Nano Lett 2002;2:447.
[13] Wang ZY, Hu J, Yu MF. Nanotechnology 2007;18:235203.
[14] Spanier JE, Kolpak AM, Urban JJ, Grinberg I, Lian OY, Yun WS, et al. Nano Lett 2006;6:735.
[15] Wang ZY, Hu J, Yu MF. Appl Phys Lett 2006;89:263119.
[16] Naumov II, Fu HX. Phys Rev Lett 2005;95:247602.
[17] Pilania G, Alpay SP, Ramprasad R. Phys Rev B 2009;80:014113.
[18] Shimada T, Tomoda S, Kitamura T. Phys Rev B 2009;79:024102.
[19] Zhang YH, Hong JW, Liu B, Fang DN. Nanotechnology 2009;20:405703.
[20] Zhang YH, Hong JW, Liu B, Fang DN. Nanotechnology 2010;21:015701.
[21] Hong JW, Fang DN. Appl Phys Lett 2008;92:012906.
[22] Hong JW, Fang DN. J Appl Phys 2008;104:064118.
[23] Morozovska AN, Eliseev EA, Glinchuk MD. Phys Rev B 2006;73:214106.
[24] Morozovska AN, Eliseev EA, Glinchuk MD. Physica B 2007;387:358.
[25] Wang JJ, Wu PP, Ma XQ, Chen LQ. J Appl Phys 2010;108:114105.
[26] Zhong WL, Wang YG, Zhang PL, Qu BD. Phys Rev B 1994;50:698.
[27] Pertsev NA, Zembilgotov AG, Tagantsev AK. Phys Rev Lett 1998;80:1988.
[28] Yamada T. J Appl Phys 1972;43:328.
[29] Wang JJ, Meng FY, Ma XQ, Xu MX, Chen LQ. J Appl Phys 2010;108:034107.
[30] Li YL, Chen LQ. Appl Phys Lett 2006;88:072905.
[31] Tagantsev AK, Gerra G. J Appl Phys 2006;100:051607.
[32] Zheng Y, Woo CH, Wang B. Nano Lett 2008;8:3131.
[33] Lin SP, Zheng Y, Cai MQ, Wang BA. Appl Phys Lett 2010;96:232904.
[34] Woo CH, Zheng Y. Appl Phys A-Mater Sci Process 2008;91:59.
[35] Zheng Y, Woo CH. Appl Phys A-Mater Sci Process 2009;97:617.
[36] Tagantsev AK. Ferroelectrics 2008;375:19.
[37] Wang J, Tagantsev AK, Setter N. Phys Rev B 2011;83:014104.
[38] Wang CL, Smith SRP. J Phys-Conden Matt 1995;7:7163.
[39] Morozovska AN, Glinchuk MD, Eliseev EA. Phys Rev B 2007;76:014102.
[40] Cottam MG, Tilley DR, Zeks B. J Phys C-Solid State Phys 1984;17:1793.
[41] Devonshire AF. Philos Magaz 1949;40:1040.
[42] Hlinka J, Márton P. Phys Rev B 2006;74:104104.
[43] Ishikawa K, Uemori T. Phys Rev B 1999;60:11841.
[44] Kay HF, Vousden P. Philos Magaz 1949;40:1019.
[45] Li YL, Cross LE, Chen LQ. J Appl Phys 2005;98:064101.

[46] Wang YL, Tagantsev AK, Damjanovic D, Setter N, Yarmarkin VK, Sokolov AI, et al. J Appl Phys 2007;101:104115.
[47] Jackson JD. New York: Springer; 1962.
[48] Morozovska AN, Eliseev EA. Taylor & Francis; 2010.
[49] Glinchuk MD, Morozovskaya AN. Phys Status Solidi B-Basic Res 2003;238:81.